SSC23-S1-04

An Ultra-Compact Ion Mass Spectrometer for Observations of Planetary Ionospheres

Carlos A. Maldonado, Gabriel Wilson, Justin McGlown, Heidi Morning, Daniel Arnold, Thomas K. Kim, Tatiana N. Espinoza, Micalah Miller, Anthony J. Rogers, Daniel Reisenfeld, and Michael Holloway

Los Alamos National Laboratory
Los Alamos, NM; 505-667-1933
cmaldonado@lanl.gov

ABSTRACT

The Compact Ion Mass Spectrometer (CIMS) is an ultra-low resource ion mass spectrometer being designed to make observations of low-energy space plasmas such as that in planetary ionospheres. The CIMS utilizes a laminated collimator to define the field-of-view, a laminated electrostatic analyzer to selectively filter ions based on energy-per-charge (*E/q*), a magnetic sector analyzer to separate ions by mass-per-charge (*M/q*), and a microchannel plate with a position sensitive cross-delay anode assembly (XDL/MCP) to detect the location of the ions on the detector plane. This ion mass spectrometer is a simple, compact, and robust instrument ideal for obtaining low-energy (0.1 eV to 1000 eV) ion composition measurements of terrestrial and planetary ionospheres. The combination of the laminated analyzer design, which creates a ribbon-like signal beam, and large area (XDL/MCP) imaging anode allows for a mass resolution (*M/ΔM)* of approximately sixteen, which is comparable to state-of-the-art ion mass spectrometers. The laminated ESA design incorporates a large number of independent analyzer elements in a grid configuration which allows for the geometric factor, i.e. instrument sensitivity, to be scaled as a function of the total number of elements. This scalability provides for custom CIMS instruments each specifically tailored for a space plasma environment. The concept and operation are intrinsically simple and enable ultrafast (~50 kHz) measurement of plasma ion composition to provide an improved understanding of the physical processes that drive complex ion dynamics in planetary ionospheres. The CIMS's low-resource constraints make it a viable candidate for implementation in missions requiring multi-point observations using satellite constellations, as a primary payload on a CubeSat platform, or as a science payload on a resource constrained spacecraft destined for planetary environments. We outline the design, simulated instrument response, and initial laboratory results of the CIMS prototype. Additionally, we then use the results from initial calibration tests and our refined electro-optic model to simulate the instrument response in the terrestrial ionosphere and in the vicinity of various planetary bodies in the local solar system.

INTRODUCTION

Ion mass spectrometers have been an integral component of heliospheric and planetary missions since the dawn of the space age – providing critical observations regarding the plasma composition, sources, sinks, and acceleration mechanisms of the terrestrial ionosphere and magnetosphere [1]. The two predominant approaches used in current space instrumentation to obtain ion composition measurements are through temporal or spatial methods. Time-of-flight (TOF) ion mass spectrometers measure the time it takes for an ion of known energy to traverse a given length and utilize, for example, thin carbon foils to trigger timing electronics [2] and linear-electric-fields (LEF) to achieve high mass resolution via time focusing [3]. These observations require additional resources such as sophisticated timing electronics, long drift regions, and high voltage power supplies. While these instruments are exquisite in both design and capability the measurement sensitivity comes at a high-cost that excludes them from smaller missions operating under ever increasing fiscal constraints or for implementation as science payloads of large constellations required for ubiquitous multi-point space plasma measurements. Ion mass spectrometers utilizing magnetic analyzers separate ions spatially by altering their trajectories based on *M/q* [4]. This design offers advantages such as it does not require numerous static or sweeping voltages which entail additional power supplies and complex electronics, as do TOF ion mass spectrometers. Disadvantages of the magnetic sector analyzer include high mass requirements for the magnetic material needed to sufficiently bend ions with energy of tens of keV. Due to the very low energy ions of planetary ionospheres of interest for the CIMS design the mass requirement is reduced.

Historically, instrument design has been guided by the philosophy of "build to performance" however the current fiscal environment of ever dwindling budgets and limited opportunities has revitalized the demand for

low-resource instruments that can yield relevant science return [5, 6, 7, 8]. Additionally, as the space physics community has developed a growing interest in the benefits of CubeSat missions, with their ability to provide spatial and temporal measurements at a reduced cost, there has been an increased focus in the development of miniaturized instruments capable of providing salient data with minimal mass, volume, and power consumption requirements. In support of this emerging trend, NASA has developed the CubeSat Launch Initiative which provides NASA a mechanism for low-cost technology development and scientific research to help bridge strategic knowledge gaps and accelerate flight-qualified technology [9].

The CIMS's low-resource constraints make it a viable candidate for implementation in missions requiring multi-point observations using satellite constellations, as a primary payload on a CubeSat platform, or as a science payload on a resource constrained spacecraft destined for planetary environments. The low-resource requirements of the CIMS instrument, in combination with the relaxed fabrication techniques and ease of assembly, allows for rapid production of a number of sensors which can then be readily added as an auxiliary payload to any number of satellite platforms to obtain the necessary observations of low-energy plasma in planetary ionospheres or the solar wind.

Notably, the National Academy of Sciences 2022 Decadal Survey of Planetary Science has identified a Uranus Orbiter as the "highest priority new Flagship mission for the decade 2023-2032". Uranus is one of the most intriguing bodies in the solar system, having an extreme axial tilt giving rise to one of the most dynamic and complex magnetospheres in the solar system. Because of the great distance to Uranus, the payload must scrupulously economize mass to reach Uranus in a reasonable time. Innovative low-resource instrument concepts such as CIMS are needed to fill the call for science observations for missions such as this.

THE CIMS INSTRUMENT OVERVIEW

The CIMS instrument is a double focusing mass spectrometer and utilizes electric and magnetic field geometries to focus in both direction and energy. This design, based on the Mattauch-Herzog geometry, allows for multiple ion species to become spatially distributed by *M/q* along the focal plane as a true mass spectrum [10]. The instrument is comprised of: (1) a laminated collimator to set the field-of-view (FOV); (2) a laminated electrostatic analyzer (ESA) to selectively filter ions by *E/q*; (3) a magnetic sector analyzer to separate ions by *M/q*; and (4) a microchannel plate (MCP) followed by position sensitive cross delay anode (XDL) assembly to detect the location of the ions on the detector plane. The CIMS instrument concept is illustrated in Figure 1.

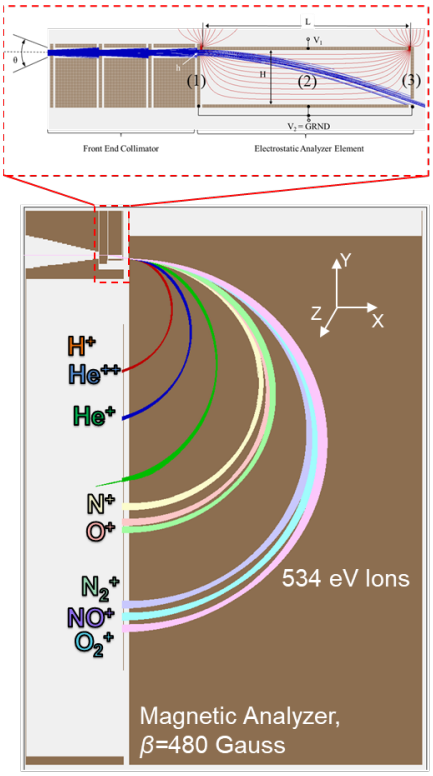

Figure 1. Magnified cross-sectional view for a single laminated electrostatic analyzer element showing the collimator, (1) the entrance aperture plate, (2) electrostatic analyzer cavity, and (3) exit aperture plate. (bottom) The complete end-to-end SIMION simulation of the CIMS discriminating ion species with incident energy of 534 eV.

Previous versions of laminated plasma spectrometers have successfully flown; however, they were constructed using high-cost silicon wafers created using microelectromechanical fabrication techniques such as deep reactive ion etching [11, 12, 13]. The CIMS laminated analyzer design uses laser etching of stainless-steel sheets and electro-discharge machining (EDM) of aluminum, tungsten, or titanium to produce extremely robust and low-cost electrostatic analyzers while maintaining high instrument performance critical to science return. The implementation of laser etched stainless steel laminated electrodes has been successfully demonstrated in a constellation of plasma spectrometers designed and developed to provide observations of ionospheric plasma and subsequent spacecraft charging [14, 15]. These previous instruments were based on a retarding potential analyzer design and are effectively high-pass energy filters. For ion mass spectroscopy applications, a narrow energy band is required therefore a prototype sensor head for CIMS was developed to act

as an ion energy bandpass filter and is shown in Figure 2 (top). The CIMS rendered mechanical design is shown in Figure 2 (bottom).

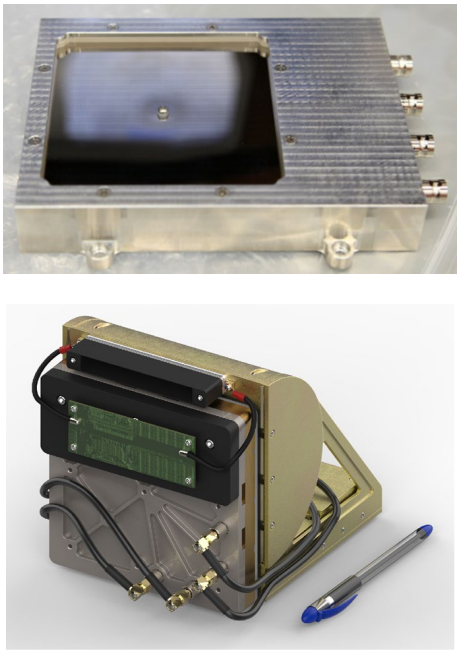

Figure 2. (top) Photograph of the CIMS prototype front-end laminated collimator and electrostatic analyzer. (bottom) Rendered CAD model of the CIMS sensor head.

Laminated Collimator and Electrostatic Analyzer Description

The baffled collimator is based on previous laminated analyzer designs such as the FlaPS [13] and Canary [12] instruments. The collimator section is necessary to reduce scatter and prevent off-angle incident ions from entering the detector in addition to preventing photons from entering the analyzer and creating background counts on the MCP [16]. A schematic of the front-end collimator and the electrostatic analyzer is shown in Figure 1 (top). After exiting the collimator, the ions enter the electric field generated between the two parallel plates of the electrostatic analyzer cavity. The ESA portion of the sensor head is based on a laminated design and is composed of three stacked conducting electrode layers with precise patterns of holes and slots machined in each layer to create several analyzer elements that consist of: (1) an entrance aperture, (2) ESA cavity, and (3) exit aperture, as depicted in the exploded CAD model in Figure 3 (top).

The entrance and exit apertures are rectangular slots with typical dimensions on the order of one hundred to several hundred microns, where height, h, is the height of the entrance aperture. The slits are laser etched in stainless steel plates and define the analyzer FOV. These slits are 100 by 200 µm. The ESA cavities are created using an EDM technique to create the internal channels depicted as region (2) shown in Figure 1. The overall channel height and length are designated H and L, respectively. The electrostatic analyzer cavity is created using interlacing aluminum fins such that the two segments biased to V_1 and V_2 are isolated from each other using thin insulating spacers and the anode is mounted downstream of the exit aperture, both of which are not shown for clarity.

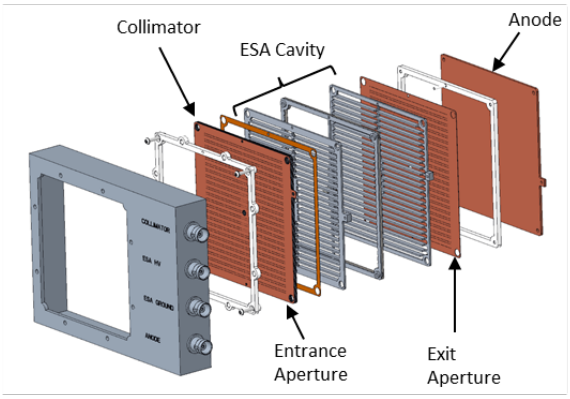

Figure 3. (top) Exploded view of the laminated electrostatic analyzer design depicting (from left to right) the entrance aperture, ESA cavity, and exit aperture layers. (bottom) hi-magnification image using Keyence microscope of the front face of the prototype sensor [17].

The electric field is created by applying a bias to the discriminator plate, V_1, while holding the opposite plate, V_2, at the host vehicle ground. In this biasing scheme V_1 is referred to as V_{ESA}. The combination of the applied electric field and analyzer geometry allow ions within a narrow range of a specified bandpass energy, $E/q = E_{set}$, to successfully travel through the entrance aperture, become deflected by the transverse electric field in the ESA cavity, and exit the cavity to enter the magnetic analyzer section as shown in Figure 1. The analyzer geometry alone determines the range of E/q accepted. Using the derivation of Feldmesser, et al. [12], the analyzer constant, k, can be calculated from the physical dimensions of the ESA

$$k = \frac{1}{4f}\left(\frac{L}{H}\right)^2 \quad (1)$$

where L is the length of the ESA, H is the center-to-center distance of the aperture openings within the ESA cavity, and $f = H/(H+h)$, as shown in Figure 1. An accurate knowledge of the analyzer constant allows for determination of the incident charged particle energy through the relationship

$$E = k \cdot V_{ESA} \quad (2)$$

where E is the streaming charged particle energy in eV and V_{ESA} is the bias voltage in volts on the ESA. Of equal importance to the analyzer constant is the energy resolution, which is the ability of the sensor to distinguish between ions of similar energy. The physical dimensions of the ESA design dictate the ideal energy resolution as follows

$$\left(\frac{\Delta E}{E}\right)_{FWHM} = \frac{4f(1-f)}{3f^2 + 2f - 1} \quad (3)$$

where $(\Delta E/E)_{\mathrm{FWHM}}$ is the energy resolution at the full width at half maximum (FWHM). The specific physical dimensions of the prototype ESA are compared to the refined CIMS ESA and the resulting analytical coefficients are listed below in Table 1. The energy resolution and analyzer constant can be adjusted to meet specific criteria through careful design of the physical parameters; however, the analytical values for these parameters require experimental characterization against a charged particle source. As with all electrostatic analyzers deviations in the physical sensor head due to machining and mechanical tolerances can lead to discrepancies between the analytical design and operational instrument response. The current analyzer constant for the CIMS ESA design requires a 150 V power supply to measure the ion energies of interest (<1 keV).

Table 1: ESA physical dimensions and analytic coefficients.

Design	*L* (µm)	*H* (µm)	*h* (µm)	*f*	*k*	$\left(\frac{\Delta E}{E}\right)_{FWHM}$
Proto-type[a]	2400	550	150	0.786	6.06	0.278
CIMS	3500	700	100	0.875	7.01	0.144

[a]This prototype refers to the proof of concept of the low-resource laminated ESA described by Maldonado [17].

Electro-optic Modeling Results

The optimization of the CIMS performance as a function of energy and mass resolution has been the focus of previous research efforts [18]. The CIMS instrument concept, illustrated in Figure 1, was modeled using the SIMION software package [19] using ion species relevant to planetary ionospheres to demonstrate the feasibility of the design. These initial results for ion species separation based on mass and charge state provide confidence that the instrument has the potential to make critical measurements of planetary ionospheres and cold magnetospheric ion populations in terms of species, energy, and flux. Modeling of the collimator and electrostatic analyzer electro-optics was conducted to provide preliminary analysis of the CIMS instrument performance in terms of the analyzer constant, energy resolution, FOV, and geometric factor. The simulations use the Monte-Carlo method to compute an isotropic input distribution over five significant input variables. The initial ion kinetic energy, particle source plane, and tangential velocity component were randomly generated within a range such that the entire response of the instrument was captured at each extreme. This method is described in detail in Collinson et al. [20].

While the laminated analyzer design is a somewhat unique plasma spectrometer design, it is at a fundamental level, deflector-type electrostatic analyzer and can therefore be characterized in terms of the classic ESA parameters. The characteristics of merit for electrostatic analyzer performance analysis are the analyzer constant, energy resolution, angular resolution, and geometric factor. Simulations using the input distribution shown previously were performed for ESA voltages (V_{ESA}) starting at 0.1 V and then for each integer voltage from 1 to 150 V. Ions that pass through the ESA cavity and exit aperture are cataloged and used to derive histograms for the number of detected ions with respect to initial ion kinetic energy and ESA plate voltage. The result for the analyzer constant, energy resolution, and acceptance angles over the projected energy range of the instrument shown are listed in Table 2.

Table 2. ESA parameters for a single analyzer element obtained from the electro-optic model.

Elevation (deg)	*Azimuth (deg)*	*GF* (cm² sr eV/eV)	*k*	$\left(\frac{\Delta E}{E}\right)_{FWHM}$
±2.3±.07	±3.1±.07	$4.8 \pm 0.2 \times 10^{-8}$	7.01	0.278

A fundamental parameter used to characterize plasma spectrometer performance is the geometric factor, *GF*, which is an effective measure of the instrument sensitivity and is a product of the collection area, energy-angle acceptancy, and efficiency of the instrument [20, 8]. The count rate is for a differential number flux F_i and species i at an energy E_j is

$$C_i(E_j) = F_i(E_j)\mathbb{GF}_{ijE}\Delta t \quad (cts/s). \quad (5)$$

The derivation and method of determining the geometric factor through ray-tracing simulation is described in detail by Collinson et al. [20] and is used here to estimate the CIMS instrument response to an isotropic input distribution,

$$\mathbb{GF}_k = \frac{C_k \Delta x \Delta y \bar{E}_D \cos^2 \bar{\theta}_D \Delta E_D \Delta \theta_D \Delta \phi}{N_{in} E_0^2}. \quad (6)$$

Where k is an index spanning ESA voltage, C_k is the number of detected ions at plate voltage k, Δy is the area

of the particle source, $\overline{E_D}$ is the mean ion kinetic energy simulated, $\overline{\theta_D}$ is the mean elevation angle, ΔE_D is the range of ion kinetic energy, θ_D is the range of simulated elevation angles, $\Delta\Phi$ is the range of simulated azimuth angles, N_{in} is the number of particles simulated, and E_0 is the mean kinetic energy of the detected distribution.

The geometric factor for a single laminated ESA element is not large, however, the laminated design allows for the fabrication of an array of many elements. The CIMS instrument is a collection of hundreds to thousands of similar channels, therefore the whole instrument geometric factor can be up to three orders of magnitude greater than the displayed value. Since the geometric factor of the individual analyzer elements is independent, any number of elements can be populated on a detector face to provide the appropriate sensitivity. Therefore, creating an "ion ribbon beam" from the CIMS ESA through the magnetic analyzer will require an array of elements that is one element tall, i.e. a single row, by 82 elements wide providing a geometric factor of 1.14 10^{-6} cm^2 sr eV/eV.

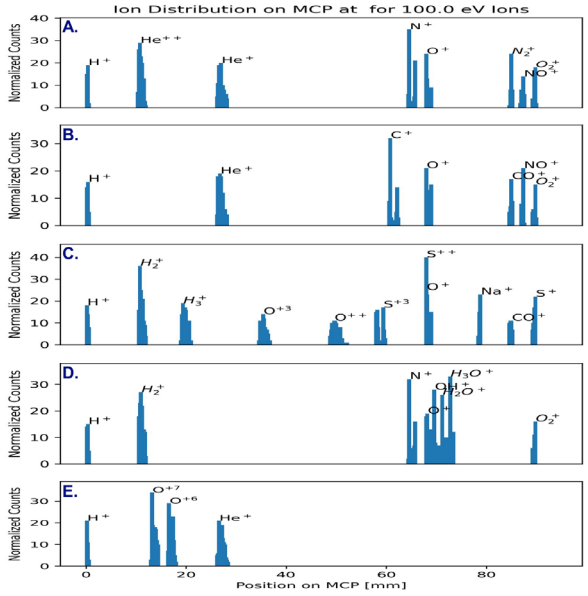

Figure 4. CIMS instrument response with regard to mass resolution at various planetary

The ability of CIMS to distinguish between ion populations found in various planetary ionospheres and regions of the solar system was modeled and shown in Figure 4. The same number of particles for each ion species population were simulated and the positions on the MCP were modeled. The locations and populations simulated were: (A) Earth, (B) Venus, (C) Jupiter – near Europa, (D) Saturn, and (E) the pristine Solar Wind. Note, SO_2^+ was also investigated for Jupiter but did not impinge on the detector. Each system was sampled using the same magnetic configuration, for a dedicated mission the instrument will be adjusted to fully sample the anticipated environment.

Analytic test results of the instrument sensitivity in various space environments are shown in Figure 5. Dashed lines are the measurement limit (i.e., one-count level of the instrument) calculated from relating equations

$$C=\varepsilon\cdot GF\cdot E\cdot j\cdot\Delta t \tag{7}$$

$$j=\frac{2E}{m^2}\cdot f \tag{8}$$

where C is counts, ε is detection efficiency, GF= 1.4×10^{-6} sr cm^2 eV/eV is the geometric factor (corresponding to 84 ESA channels), E is energy ranging from 1 eV/q to 10 keV/q, j is flux, Δt=1s is the instrument duty cycle, and f is phase space density. Solid lines are the realistic plasma distribution at (A) the ionosphere of Venus, (B) Jupiter's magnetosphere, and (C & D) the terrestrial ionosphere with/without spacecraft potential (Φ_{SC}=–10V). Incorporating the spacecraft potential is an essential part in understanding the energy distributions of low-energy ionospheric ions. Spacecraft operating in the Earth's ionosphere develop negative spacecraft potential which then accelerates ions to spacecraft and detector surfaces. This acceleration mechanism has been shown to have an impact on ion trajectories, energy distribution measurements, and resulting moments [21, 22]. These test results show that CIMS has adequate instrument sensitivity and energy range to measure both ionospheric and magnetospheric ions within terrestrial and planetary magnetospheres. Plasma distributions were obtained from Dougherty et al. [23], Bilitza et al. [24], Miller and Whitten [25], and Wilson et al. [26].

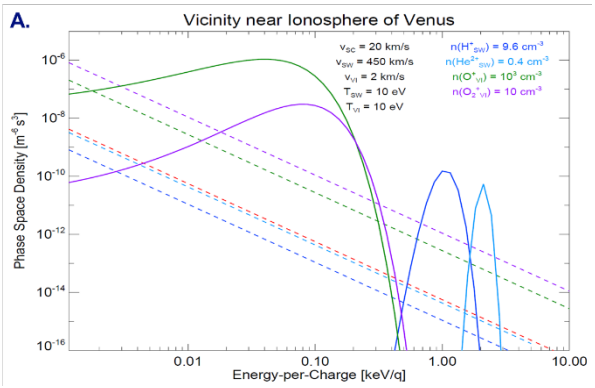

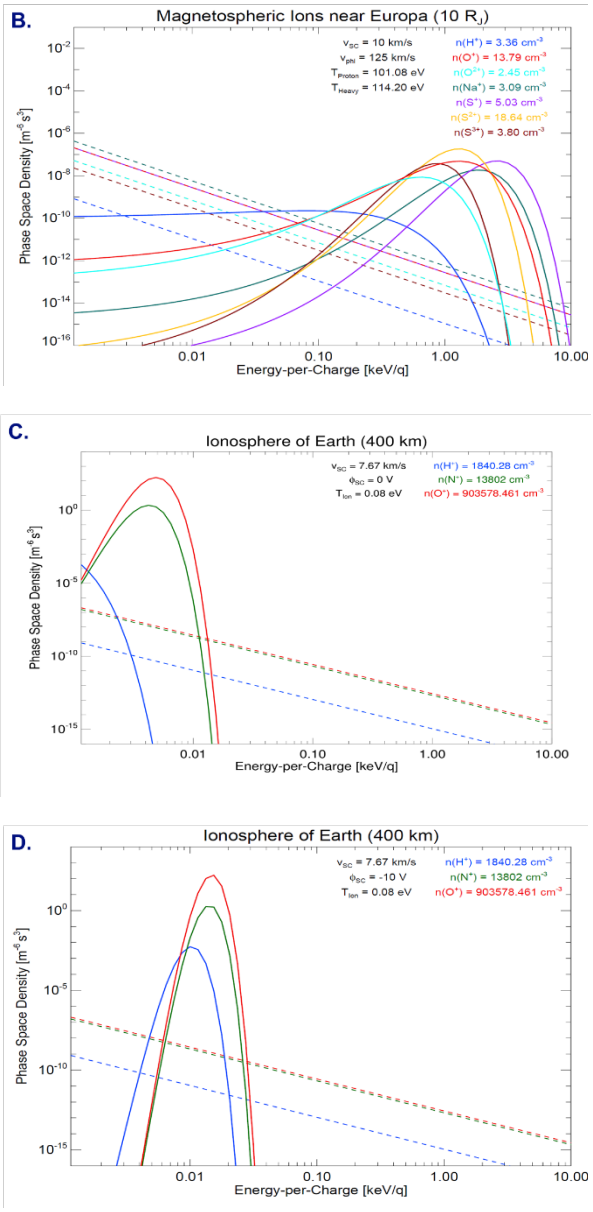

Figure 5. Analytic test results of the instrument sensitivity in various space environments. Dashed lines indicate measurement limit of the instrument and solid lines are known ion phase space density distributions. CIMS can properly measure the bulk ion distribution.

Initial Laminated ESA Results

The CIMS laminated collimator and ESA sensor front-end was tested against a low energy plasma source in an effort to simulate the low-Earth orbit (LEO) plasma environment where satellites and spacecraft regularly charge to negative potentials [27]. The testing was conducted using a transverse magnetic filter plasma source capable of simulating the Earth's ionospheric environment. The source produces streaming ions with energy of approximately 2-5 eV and a low electron temperature of approximately 0.2 eV [28, 29]. The density of the plasma produced is between 1.4×10^6 and 4.4×10^7 cm^{-3} when measured at a distance of 1 meter downstream from the source [30].

The ESA was mounted to a 0.4 m square aluminum plate to simulate the instrument being mounted to a spacecraft panel. Measurements were conducted while biasing the plate at seven different spacecraft voltages with the sensor head ground referenced to the plate voltage. The distance between the sensor head and exit aperture of the plasma source was 0.25 m, as shown in Figure 6.

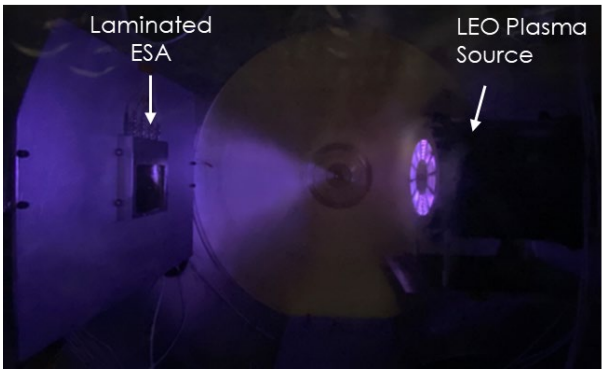

Figure 6. Photograph of the laminated collimator and ESA front-end during testing against the LEO plasma source.

These initial tests were used to experimentally determine the analyzer constant and evaluate the ability of the CIMS front-end sensor to monitor spacecraft charge. The plasma source was operated at a flow rate of 10 sccm Argon, with anode current and voltage of 7.5 A and 31 V, respectively. The streaming ion energy was measured using a retarding potential analyzer (RPA) prior to conducting ESA measurements to provide a baseline comparison. The RPA measurements returned an ion energy of 3.2 eV at the specified source operating parameters. An external power supply was used to bias the instrument such that the ground reference for the sensor could be set to a negative potential, thus simulating a negative spacecraft frame charge. The measured ESA distributions as a function of the increasing negative applied bias from -10 to -35 V are shown in Figure 9 from left to right. The total energy peaks are well defined and increase as expected due to the additional energy imparted to the incident ions as they passed through the potential difference between the plasma field and the ESA ground reference.

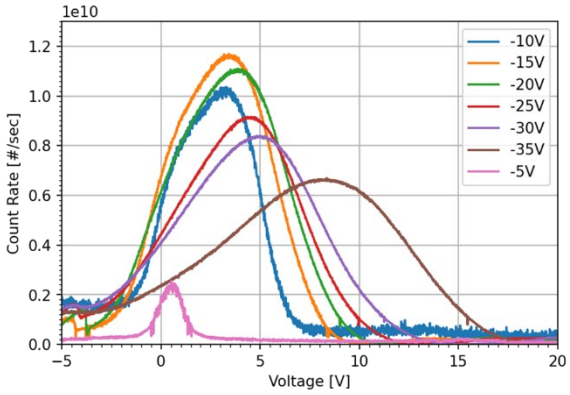

Figure 7. ESA measurements as a function of simulated spacecraft bias.

The analyzer constant was determined by using the combined magnitude of the streaming ion energy and applied spacecraft bias to obtain the total energy and is shown in Figure 8. For example, at -10 V applied spacecraft bias, the ESA should measure 13.2 eV ions. The average analyzer constant from -10 to -30 V applied spacecraft bias is 6.0 ± 0.05. The values at -5 and -35 V were excluded as outliers. Future work will include a minimum of ten measurements at each applied spacecraft bias to reduce the effect of outliers and obtain standard deviations for measurements.

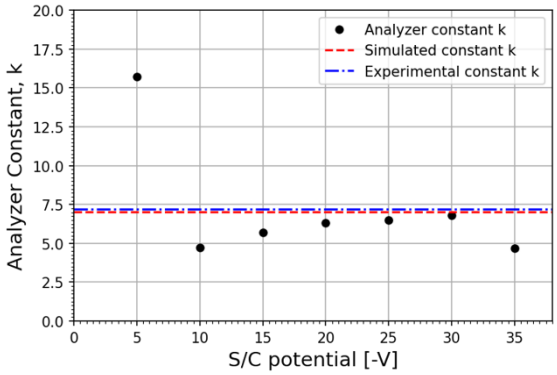

Figure 8. Analyzer constant as a function of simulated spacecraft bias.

The experimental (7.01) and simulation (5.8 ± 0.5) determined analyzer constants were then applied to the ESA measurements shown in Figure 7 to convert to energy. The linear blue line indicates the anticipated total ion energy of 3.2 eV plus the additional acceleration due to the applied spacecraft bias. While the initial ESA data follow a similar trend, additional measurements are needed to obtain standard deviations and assess error.

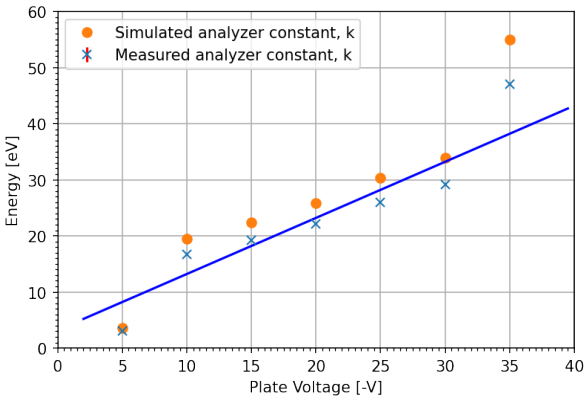

Figure 9. ESA measurements converted to energy using the experimental and simulation determined analyzer constants.

Magnetic Analyzer Section

A magnetic analyzer section, created utilizing samarium-cobalt permanent magnets, will be positioned downstream of the electrostatic analyzer to separate ions based on momentum-to-charge, *M/q*. The low-energy range of the CIMS results in a reduced magnetic field strength requirement and therefore less magnetic material for a low-resource instrument profile. Ions will exit the electrostatic analyzer section within a narrow range of the selected bandpass energy and be post-accelerated by 3 kV using an electroformed nickel mesh grid. The ions will then enter the magnetic analyzer section and the ion trajectories will subsequently diverge based on *M/q* such that high-mass ions will be deflected less than lighter species such as H^+.

The initial design of the magnetic analyzer shape has been created in SIMION using several "pixels" that are parallel square magnetic poles with the field line pointing into the image (z-axis) as shown in Figure 1. The magnetic sector field strength has been optimized at ~450-480 Gauss to focus high mass ions (16 amu) onto the detector plane. This will provide the best mass resolution possible to resolve between N^+ and O^+ across the entire energy range of the instrument. Note, this is ideal for observations of the Earth's ionosphere and can be tuned based on the target destination.

Future modeling efforts will focus on creating a more refined geometry in SIMION to create a curved radius at the outermost edge of the magnetic analyzer section. This radius will be defined by the trajectory of the heaviest ion with the highest energy to be measured by the CIMS. Removing the unnecessary magnetic material will provide mass reduction. The magnetic sector will be created using samarium cobalt or neodymium boron iron

magnets depending on temperature requirements and will be fabricated by Plasma Controls, LLC according to the physical dimensions and field strength requirements derived from the SIMION modeling analysis. Plasma Controls, LLC has extensive experience utilizing magnetic fields created using permanent magnets to generate unique plasma sources, advanced spacecraft propulsion systems, and plasma diagnostics [29, 31].

Position Sensitive Cross-Delay Anode

The location of the ions incident on the detector plane will be observed using an MCP stack followed by an XDL anode. Plasma spectrometer detectors typically require a particle count rate maximum of 10^5 s^{-1} and detector speed <100 ns per event to prevent pulse pile-up [32]. The XDL sensors operate at a specified detection rate of $>10^6$ s^{-1} with a timing accuracy of 0.1 ns FWHM and spatial resolution of 35 µm FWHM. These parameters have been identified as more than sufficient for plasma spectrometers and a reduced performance version of the XDL anode is currently being investigated as the detector plane for a flight version of the Wide field-of-view Plasma Spectrometer (WPS) [33, 34, 35, 36]. The XDL sensors have an established history of use in space-based instruments for photon detection [37, 38, 39, 40, 41]. LANL has flown 1-D versions of this technology on LANL instruments or subsystems on the IMAGE [42] and TWINS [43] missions.

The XDL assembly consists of a standard MCP detector in a z-stack (3 plate) configuration followed by a cross delay-line anode. An incident ion strikes the front of the MCP detector and generates a secondary electron avalanche, resulting in a gain of ~10^7, which exits the MCP depositing the resulting charge on the anode [44]. The XDL anode is formed by two orthogonal serpentine conductors and the position of the charge pulse is then determined by the difference in arrival time of the pulse at the ends of resistive-capacitance delay lines, shown schematically in Figure 10. The XDL electronics consist of a high gain-bandwidth product operational amplifiers and fast comparators configured in a constant fraction discriminator (CFD) topology at the end of each delay line. This circuit amplifies the pulses from the XDL and translates the analog pulse to a digital signal to drive the start and stop inputs on the time-to-digital converter (TDC) integrated circuits. The advantage of utilizing CFD topology is to negate the effects of conventional threshold triggering which inherently introduces errors in timing measurements between analog input pulses of varying amplitudes. The CFD circuit behaves as an amplitude-invariant mechanism to drive the TDCs. The resolution of the assembly will be determined by the event timing error which is dominated by the CFD performance [45]. An initial XDL sensor with dimensions of 94 mm × 94 mm has been selected for the CIMS prototype with the majority of the electronics work being dedicated to the design and optimization of the supporting electronics. This includes the selection of necessary amplifiers and comparators for the CFD circuit, TDCs, board layout, and testing. A field-programmable-gate array (FPGA) will interface the TDCs through a SPI interface to record the start-stop events to translate to precision spatial resolution. Depending on the prototype electronics' subsequent position and time resolution, design simplification will occur to further decrease the required cost and power resources for future flight opportunities of the CIMS.

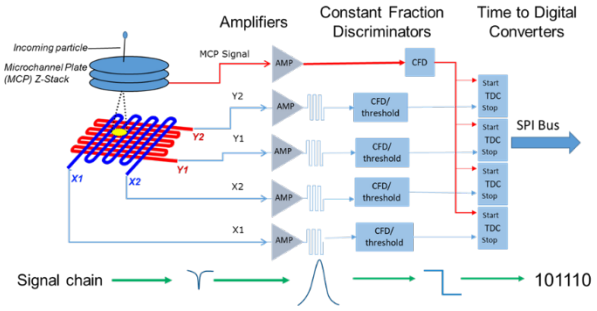

Figure 10. XDL/MCP anode assembly and electronics functional schematic.

CONCLUSIONS

We present a compact ion mass spectrometer capable of high-mass resolution for low-energy space plasma. CIMS is capable of measuring ion flux, energy, and mass for providing unique measurements of ionospheric plasma throughout the solar system. The CIMS sensor incorporates a collimator to set the FOV, a laminated electrostatic analyzer to selectively filter ions by *E/q*, a magnetic sector analyzer to separate ions by *M/q*, and a position-sensitive XDL/MCP 2-D imaging anode to provide low-energy ion composition measurements. The objective of the CIMS is to provide sufficient energy resolution, geometric factor, mass range, and mass resolution when compared to current state-of-the-art ion mass spectrometers, coupled with significant reductions in mass, volume, and power requirements. This comparable performance with reduced resources is accomplished by designing to a narrower operational energy range (0-1000 eV) to focus on ion composition measurements of low-energy planetary ionospheres. Based on the initial CIMS electro-optic models and heritage subsystems of iMESA and TWINS, we estimate that the resources for a flight CIMS (including XDL/MCP electronics and power supplies) are approximately 5 kg, 4.8 W (including high voltage power supply draw), and less than 1000 cm^3.

Additionally, the analyzer constant for the CIMS ESA design requires only a 150 V power supply to measure the ion energies of interest (<1 keV), thus minimizing stepping high voltage power supply requirements. Electro-optic modeling of the CIMS collimator and ESA elements indicate energy resolution of 29% and a geometric factor on the scale of similar instruments, 1.97×10^{-5} sr cm^2 eV/eV, however with lower size, weight, and power. These initial electro-optic results for ion species separation based on mass and charge state provide confidence that the instrument has the potential to make critical measurements of planetary ionospheres and cold magnetospheric ion populations in terms of species, energy, and flux.

Future work will include continuing characterization of the laminated collimator and ESA using an electron beam with an additional design iteration to improve energy resolution and geometric factor. End-to-end simulations of the CIMS instrument will allow for further optimization of the magnetic filter and subsequent mass resolution. Optimization will be considered successful when the energy resolution and mass resolution of the instrument is sufficient to characterize these individual ion species distributions throughout the full energy range of the instrument.

Acknowledgments

This work was funded through the NASA H-TIDS award 80HQTR21T0062. The research conducted at Los Alamos National Laboratory was under the auspices of the Department of Energy. LANL is operated by Triad National Security, LLC, for the National Nuclear Security Administration of U.S. Department of Energy (DOE) (Contract No. 89233218CNA000001).

References

[1] C. Maldonado, P. Resendiz Lira, G. Delzanno, B. Larsen, D. B. Reisenfeld and V. Coffey, "A review of instrument techniques to measure magnetospheric cold electrons and ions," *Frontiers in Astronomy and Space Sciences,* vol. 9, 2023.

[2] D. McComas, F. Allegrni, C. Pollock, H. Funsten, S. Ritzau and G. Gloeckler, "Ultrathin (~10 nm) carbon foils in space instrumentation," *Rev. Sci. Instrum.,* vol. 75, no. 11, p. 4863–4870, 2004.

[3] D. McComas, J. Nordholt, S. Bame, B. Barraclough and J. Gosling, "Linear electric field mass analysis: a technique for three-dimensional high mass resolution space plasma composition measurements," *Proc. Natl. Acad. Sci. USA,* vol. 87, pp. 5925-5929, 1990.

[4] H. Balsiger, A. Altwegg, P. Bochsler, P. Eberhardt, J. Fischer, S. Graf, A. Jackel, E. Kopp, U. Langer, M. Mildner, J. Muller, T. Riesen, M. Rubin, S. Scherer, P. Wurz, S. Wuthrich, E. Arijs, S. Delanoye, J. De Keyser, E. Neefs, D. Nevejans and H. Reme, "ROSINA - Rosetta orbiter spectrometer for ion and neutral analysis," *Space Sci. Rev.,* vol. 128, pp. 745-801, 2007.

[5] D. Young, "Space plasma particle instrumentation and the new paradigm: Faster, cheaper, better," in *Measurement Techniques in Space Plasmas: Particles*, R. Pfaff, J. Borovsky and D. Young, Eds., Geophysical Monograp Series 102, 1998, pp. 1-16.

[6] E. MacDonald, H. Funsten, E. Dors, M. Thomsen, P. Janzen, R. Skoug, G. Reeves, J. Stenberg, R. Harper, D. Young, J.-M. Jahn and D. Reisenfeld, "New Magnetospheric Ion Composition Measurement Techniques," 2009.

[7] P. Fernandes, H. Funsten, E. Dors, R. B. Harper, E. MacDonald, D. Reisenfeld, R. Skoug, J. Steinberg and M. Thomsen, "Low-Resource Technique for Measurement of H+ and O+ in the Terrestrial Magnetosphere," *J. Geophys. Res.:Space Physics,* vol. 124, p. 9137–9153, 2019.

[8] H. Funsten and D. McComas, "Limited resource plasma analyzers:Miniaturization concepts," in *Measurement Techniques in Space Plasmas: Particles*, R. Pfaff, J. Borovsky and D. Young, Eds., AGU Monograph Series, 1998, pp. 157-167.

[9] NASA, "CubeSat Launch Initiative," 2020. [Online]. Available: https://www.nasa.gov/directorates/heo/home/CubeSats_initiative. [Accessed 28 August 2020].

[10] J. Mauttach and R. Herzog, "Uber einen neuen Massenspektrographen," *Z. Phys.,* vol. 89, pp. 786-795, 1934.

[11] C. Maldonado, M. McHarg, R. Balthazor and R. Osiander, "Undergraduate research and science

mission opportunities with microtechnology enabled particle detectors," in *Proc. SPIE 10982, Micro- and Nanotechnology Sensors, Systems, and Applications XI, 109820I*, Baltimore, 2019.

[12] H. Feldmesser, M. Darrin, R. Osiander, L. Paxton, A. Rogers, J. Marks, M. McHarg, R. Balthazor, L. Krause and J. Fitzgerald, "Canary: ion spectroscopy for ionospheric sensing," in *Proc. SPIE, Space Missions and Technologies*, Orlando, FL, United States, 2010.

[13] D. M. Wesolek, J. L. Champion, F. A. Herrero, R. Osiander and R. L. Champion, "A micromachined flat plasma spectrometer," in *Proc. SPIE 5344, MEMS/MOEMS Components and their Applications*, 2004.

[14] C. Maldonado, R. Cress, P. Gresham, J. Armstrong, G. Wilson, D. Reisenfeld, B. Larsen, R. Balthazor, J. Harley and M. McHarg, "Space radiation dosimetry using the integrated Miniaturized Electrostatic Analyzer - Reflight (iMESA-R)," *Space Weather,* 2020.

[15] G. McHarg, P. Neal, N. Taormina, A. Strom and R. Balthazor, "USAFA Integrated Miniaturized Electrostatic Analyzer (iMESA) - An Undergraduate Space Weather Constellation," *Space Weather,* vol. 13, pp. 827-830, 2015.

[16] T. H. Zurburchen, P. Bochsler and F. Scholze, "Reflection of ultraviolet light at 121.6 nm from rough surfaces," *Optical Engineering,* vol. 34, no. 5, 1995.

[17] C. A. Maldonado, Z. Eyler, B. Pierce, L. Matson, P. Neal, H. Richards, R. L. Balthazor, J. Harley and M. G. McHarg, "A laminated energetic electrostatic analyzer for 0-5 keV charged particles," *Rev. Sci. Instrum.,* vol. 91, no. 1, 2020.

[18] C. Maldonado, G. Wilson, J. McGlown, H. Morning, D. Arnold, D. Reisenfeld and M. Holloway, "An Ultra-Low Resource Ion Mass Spectrometer for CubeSat Platforms," in *Proceedings of the 36th Annual Small Satellite Conference*, Logan, UT, 2021.

[19] D. Dahl, "SIMION for the personal computer in reflection," *Int. J. Mass Spectrom.,* vol. 200, no. 3, 2000.

[20] G. Collinson, J. Dorelli, L. Avanov, G. Lewis, T. Moore, C. Pollock, D. Kataria, R. Bedington, C. Arridge, D. Chornay, U. Gliese, A. Mariano, A. Barrie, C. Tucker, C. Owen, A. Walsh, M. Shappirio and M. Adrian, "The geometric factor of electrostatic plasma analyzers: A case study from the Fast Plasma Investigation for the Magnetospheric Multiscale mission," *Rev. Sci. Instrum.,* vol. 83, no. 3, 2012.

[21] C. A. Maldonado, D. Reisenfeld, P. Fernandes, B. Larsen, G. Wilson, R. L. Balthazor and M. G. McHarg, "The effects of spacecraft potential on ionospheric plasma measurements," *Journal of Spacecraft and Rockets,* vol. (submitted), 2020.

[22] E. E. Scime, J. L. Phillips and S. J. Bame, "Effects of spacecraft potential on three-dimensional electron measurements in the solar wind," *J. of Geophys. Res.,* vol. 99, no. A8, pp. 14,769-14,776, 1994.

[23] D. L. P., K. M. Bodisch and F. Bagenal, "Survey of Voyager plasma science ions at Jupiter:," *Journal of Geophysical Research: Space Physics,* vol. 122, pp. 8257-8276, 2017.

[24] D. Bilitza, A. Altadill, V. Truhlik, V. Shubin, I. Galkin, B. Reinisch and X. Huang, "International Reference Ionosphere 2016: From ionospheric climate to real-time weather predictions," *Space Weather,* vol. 15, pp. 418-429, 2017.

[25] K. L. Miller and R. C. Whitten, "Ion dynamics in the Venus ionosphere," *Space Science Reviews,* vol. 55, pp. 165-199, 1991.

[26] L. B. Wilson III, M. L. Stevens, J. C. Kasper, K. G. Klein, B. A. Maruca, S. D. Bale, T. A. Bowen, M. P. Pulupa and C. S. Salem, "The statistical properties of solar wind temperature parameters near 1 AU," *The Astrophysical Journal Supplement Series,* vol. 236, no. 2, 2018.

[27] H. B. Garrett and A. C. Whittlesey, "Spacecraft Charging, An Update," *IEEE Transactions on Plasma Science,* vol. 28, no. 6, 2000.

[28] C. L. Enloe, L. H. Krause, M. G. McHarg, O. Nava, P. B. Shoemaker and J. D. Williams, "Characterization of a plasma source for ground-based simulation of LEO plasma conditions," in *2nd Annual International Energy Conversion Conference*, 2004.

[29] C. Maldonado, L. Rand, K. Xie, A. Ketsdever, C. Farnell and J. Williams, "Development of a magnetically filtered atomic oxygen plasma source: LEO drag applications," San Diego, California, USA, 2014.

[30] B. Rubin, C. Farbell, J. Williams, J. Vaughn, T. Schneider and D. Ferguson, "Magnetic filter type plasma source for ground-based simulation of low earth orbit environment," *Plasma Sources Sci. and Technol.,* vol. 18, 2009.

[31] Plasma Controls, "ExB Probe Wien Velocity Filter," 2020. [Online]. Available: https://www.plasmacontrols.com/exb-velocity-filter.html. [Accessed 28 August 2020].

[32] R. M. Skoug, H. O. Funsten, E. Mobius, R. W. Harper, K. H. Kihara and J. S. Bower, "A wide field of view plasma spectrometer," *J. Geophys. Res. Space Physics,* vol. 121, pp. 6590-6601, 2016.

[33] C. A. Maldonado et al., "Development of the Experiment for Space Radiation Analysis (ESRA) CubeSat Mission to GTO," in *IEEE Aerospace Conference*, Big Sky, MT, 2023.

[34] C. A. Maldonado et al., "The Experiment for Space Radiation Analysis (ESRA) - Technology Maturation of Next Generation Charged Particle Detectors in GTO," in *Advanced Maui Optical and Space Technologies (AMOS) Conference*, Maui, HI, 2022.

[35] C. A. Maldonado et al., "The Experiment for Space Radiation Analysis: Probing the Earth's Radiation Belts Using a CubeSat Platform," in *Proceedings of the 36th Annual Small Satellite Conference*, Logan, UT, 2022.

[36] C. A. Maldonado, J. Deming, B. N. Mosley, K. S. Morgan, J. McGlown, A. Nelson, P. Fernandes, M. Kroupa, K. Katko, M. P. HHehlen, D. Arnold, J. Barney, C. Safi, M. Pyle, T. Schultz, D. Reisenfeld, R. Skoug, A. Guider, M. Holloway, H. Morning, E. Krause, B. Sandoval, D. Beckman, Z. Miller, R. Merl, P. S. Graham, T. P. White, Z. Tripp, B. Hoose, C. Roecker, A. Klimenko, R. Dutch, K. Kaufeld, E. Cox, Q. Cole, C. Clanton, P. Bloser, B. A. Larsen, T. Fairbanks, J. George and J. Michel, "The Experiment for Space Radiation Analysis: A 12U CubeSat to Explore the Earth's Radiation Belts," in *IEEE Aerospace Conference*, Big Sky, MT, 2022.

[37] O. Siegmund, M. Gummin, J. Stock, G. Naletto, G. Gaines, R. Raffanti, J. S. Hull, R. Abiad, T. Rodriguez-Bell, T. Magoncelli, P. Jelinsky, W. Donakowski and K. Kromer, "Performance of the double delay line microchannel plate detectors for the Far-Ultraviolet Spectroscopic Explorer," in *Proc. SPIE 3114, EUV, X-Ray, and Gamma-Ray Instrumentation for Astronomy VIII*, San Diego, CA, 1997.

[38] J. Stock, O. Siegmund, J. Hull, K. Kromer, S. Jelinsky, H. Heetderks, M. Lampton and S. Mende, "Cross-delay-line microchannel plate detectors for the Spectrographic Imager on the IMAGE satellite," in *Proc. SPIE 3445, EUV, X-Ray, and Gamma-Ray Instrumentation for Astronomy IX*, San Diego, CA, United States, 1998.

[39] O. Siegmund, M. Gummin, T. Sasseen, P. Jelinsky, G. Gaines, J. Hull, J. Stock, M. Edgar, B. Welsh, S. Jelinsky and J. Vallerga, "Microchannel plates for the UVCS and SUMER instruments on the SOHO satellite," in *Proc. SPIE 2518, EUV, X-Ray, and Gamma-Ray Instrumentation for Astronomy VI*, San Diego, CA, United States, 1995.

[40] J. Vallerga, J. Zaninovich, B. Welsh, O. Siegmund, J. McPhate, J. Hull, G. Gaines and D. Buzasi, "The FUV detector for the cosmic origins spectrograph on the Hubble Space Telescope," *Nuclear Instruments and Methods in Physics*

Research, Section A, vol. 477, no. 1-3, pp. 551-555, 2002.

[41] O. Siegmund, P. Jelinsky, J. Stock, J. Hull, D. Doliber, J. Zaninovich, A. Tremsin and K. Kromer, "High resolution cross delay line detectors for the GALEX mission," in *Proc. SPIE 3765, EUV, X-Ray, and Gamma-Ray Instrumentation for Astronomy X*, Denver, CO, United States, 1999.

[42] C. Pollock, A. Asamura, J. Baldonado, M. Balkey, P. Barker, J. Burch, E. Korpela, J. Cravens, G. Dirks, M.-C. Fok, H. Funsten, M. Grande, M. Gruntman, J. Hanley, J.-M. Jahn, M. Jenkins, M. Lampton, M. Marckwordt, D. McComas, T. Mukai and G. Penegor, "Medium Energy Neutral Atom (MENA) Imager for the Image Mission," *Space Sci. Rev.,* vol. 91, no. 1-2, pp. 113-154, 2000.

[43] D. McComas, F. Allegrini, J. Baldonado, B. Blake, P. Brandt, J. Burch, J. Clemmons, W. Crain, D. Delapp, R. DeMajistre, D. Everett, H. Fahr, L. Friesen, H. Funsten, J. Goldstein, M. Gruntman, R. Harbaugh, R. Harper, H. Henkel, C. Holmlund, G. Lay, D. Mabry, D. Mitchell, U. Nass, C. Pollock, S. Pope, M. Reno, S. Ritzau, E. Roelof, E. Scime, M. Sivjee, R. Skoug, T. Sotirelis, M. Thomsen, C. Urdiales, P. Valek, K. Viherkanto, S. Weidner, T. Ylikorpi, M. Young and J. Zoennchen, "The Two Wide-angle Imaging Neutral-atom Spectrometers (TWINS) NASA Mission-of-Opportunity," *Space Sci Rev,* vol. 142, p. 157–231, 2009.

[44] O. Siegmund, B. Welsh, J. Vallerga, A. Tremsin and J. McPhate, "High-Performance microchannel plate imaging photon counters for spaceborne sensing," in *Proc SPIE 6220, Spaceborne Sensors III, 622004*, Orlando, FL, USA, 2006.

[45] O. Siegmund, M. Gummin, J. Stock, D. Marsh, R. Raffanti and J. Hull, "High-resolution monolithic delay-line readout techniques for two dimensional microchannel plate detectors," San Diego, CA, United States, 1993.